DTU Library

Cross-correlated imaging of single-mode photonic crystal rod fiber with distributed mode filtering

Laurila, Marko; Barankov, Roman; Jørgensen, Mette Marie; Alkeskjold, Thomas Tanggaard; Broeng, Jes; Lægsgaard, Jesper; Ramachandran, Siddharth

Link back to DTU Orbit

Cross-correlated imaging of single-mode photonic crystal rod fiber with distributed mode filtering

Marko Laurila,[1,*] Roman Barankov,[2] Mette M. Jørgensen,[1] Thomas T. Alkeskjold,[3] Jes Broeng,[1,3] Jesper Lægsgaard,[1] and Siddharth Ramachandran[2]

[1]*DTU Fotonik, Department of Photonics Engineering, Technical University of Denmark, 2800 Kgs. Lyngby, Denmark*
[2]*Photonics Center, Department of Electrical and Computer Engineering, Boston University, 8 Saint Mary's Street, Boston, Massachusetts 02215, USA*
[3]*NKT Photonics, Blokken 84, 3460 Birkerød, Denmark*
*malau@fotonik.dtu.dk

Abstract: Photonic crystal bandgap fibers employing distributed mode filtering design provide near diffraction-limited light outputs, a critical property of fiber-based high-power lasers. Microstructure of the fibers is tailored to achieve single-mode operation at specific wavelength by resonant mode coupling of higher-order modes. We analyze the modal regimes of the fibers having a mode field diameter of 60 μm by the cross-correlated (C^2) imaging method in different wavelength ranges and evaluate the sensitivity of the modal content to various input-coupling conditions. As a result, we experimentally identify regimes of resonant coupling between higher-order core modes and cladding band. We demonstrate a passive fiber design in which the higher-order modal content inside the single-mode guiding regime is suppressed by at least 20 dB even for significantly misaligned input-coupling configurations.

©2013 Optical Society of America

OCIS codes: (060.2270) Fiber characterization; (060.4005) Microstructured fibers.

References and links

1. D. J. Richardson, J. Nilsson, and W. A. Clarkson, "High power fiber lasers: current status and future perspectives [Invited]," J. Opt. Soc. Am. B **27**(11), B63–B92 (2010).
2. J. Limpert, O. Schmidt, J. Rothhardt, F. Röser, T. Schreiber, A. Tünnermann, S. Ermeneux, P. Yvernault, and F. Salin, "Extended single-mode photonic crystal fiber lasers," Opt. Express **14**(7), 2715–2720 (2006).
3. A. Galvanauskas, M. C. Swan, and C.-H. Liu, "Effectively single-mode large core passive and active fibers with chirally coupled-core structures," paper CMB1, CLEO/QELS, San Jose (2008).
4. L. Dong, H. A. Mckay, A. Marcinkevicius, L. Fu, J. Li, B. K. Thomas, and M. E. Fermann, "Extending effective area of fundamental mode in optical fibers," J. Lightwave Technol. **27**(11), 1565–1570 (2009).
5. F. Jansen, F. Stutzki, H. J. Otto, M. Baumgartl, C. Jauregui, J. Limpert, and A. Tünnermann, "The influence of index-depressions in core-pumped Yb-doped large pitch fibers," Opt. Express **18**(26), 26834–26842 (2010).
6. T. T. Alkeskjold, M. Laurila, L. Scolari, and J. Broeng, "Single-mode ytterbium-doped Large-Mode-Area photonic bandgap rod fiber amplifier," Opt. Express **19**(8), 7398–7409 (2011).
7. J. W. Nicholson, J. M. Fini, A. M. DeSantolo, E. Monberg, F. DiMarcello, J. Fleming, C. Headley, D. J. DiGiovanni, S. Ghalmi, and S. Ramachandran, "A higher-order-mode Erbium-doped-fiber amplifier," Opt. Express **18**(17), 17651–17657 (2010).
8. M. Laurila, M. M. Jørgensen, K. R. Hansen, T. T. Alkeskjold, J. Broeng, and J. Lægsgaard, "Distributed mode filtering rod fiber amplifier delivering 292W with improved mode stability," Opt. Express **20**(5), 5742–5753 (2012).
9. M. Laurila, J. Saby, T. T. Alkeskjold, L. Scolari, B. Cocquelin, F. Salin, J. Broeng, and J. Lægsgaard, "Q-switching and efficient harmonic generation from a single-mode LMA photonic bandgap rod fiber laser," Opt. Express **19**(11), 10824–10833 (2011).
10. F. Jansen, F. Stutzki, H.-J. Otto, T. Eidam, A. Liem, C. Jauregui, J. Limpert, and A. Tünnermann, "Thermally induced waveguide changes in active fibers," Opt. Express **20**(4), 3997–4008 (2012).
11. F. Stutzki, F. Jansen, A. Liem, C. Jauregui, J. Limpert, and A. Tünnermann, "26 mJ, 130 W Q-switched fiber-laser system with near-diffraction-limited beam quality," Opt. Lett. **37**(6), 1073–1075 (2012).

12. M. C. Swan, C. Liu, D. Guertin, N. Jacobsen, K. Tankala, and A. Galvanauskas, "33μm Core Effectively Single-Mode Chirally-Coupled-Core Fiber Laser at 1064-nm," in Optical Fiber Communication Conference and Exposition and The National Fiber Optic Engineers Conference, OSA Technical Digest (CD) (Optical Society of America, 2008), paper OWU2.

13. T. Eidam, J. Rothhardt, F. Stutzki, F. Jansen, S. Hädrich, H. Carstens, C. Jauregui, J. Limpert, and A. Tünnermann, "Fiber chirped-pulse amplification system emitting 3.8 GW peak power," Opt. Express **19**(1), 255–260 (2011).

14. J. W. Nicholson, S. Ramachandran, S. Ghalmi, M. F. Yan, P. Wisk, E. Monberg, and F. V. Dimarcello, "Propagation of femtosecond pulses in large-mode-area, higher-order-mode fiber," Opt. Lett. **31**(21), 3191–3193 (2006).

15. S. Ramachandran, J. M. Fini, M. Mermelstein, J. W. Nicholson, S. Ghalmi, and M. E. Yan, "Ultra-large effective-area, higher-order mode fibers: a new strategy for high-power lasers," Laser Photonics Rev. **2**(6), 429–448 (2008).

16. A. E. Siegman, "New developments in laser resonators," Proc. SPIE **1224**, 2–14 (1990).

17. A. E. Siegman, "Defining, measuring, and optimizing laser beam quality," Proc. SPIE **1868**, 2–12 (1993).

18. S. Wielandy, "Implications of higher-order mode content in large mode area fibers with good beam quality," Opt. Express **15**(23), 15402–15409 (2007).

19. J. W. Nicholson, A. D. Yablon, S. Ramachandran, and S. Ghalmi, "Spatially and spectrally resolved imaging of modal content in large-mode-area fibers," Opt. Express **16**(10), 7233–7243 (2008).

20. J. W. Nicholson, A. D. Yablon, J. M. Fini, and M. D. Mermelstein, "Measuring the modal content of large-mode-area fibers," IEEE J. Sel. Top. Quantum Electron. **15**(1), 61–70 (2009).

21. T. Kaiser, D. Flamm, S. Schröter, and M. Duparré, "Complete modal decomposition for optical fibers using CGH-based correlation filters," Opt. Express **17**(11), 9347–9356 (2009).

22. D. N. Schimpf, R. A. Barankov, and S. Ramachandran, "Cross-correlated (C^2) imaging of fiber and waveguide modes," Opt. Express **19**(14), 13008–13019 (2011).

23. R. A. Barankov, "Cross-correlation imaging for waveguide characterization", M.S. Thesis, *http://arxiv.org/abs/1206.0666v1* [physics.optics]

24. M. M. Jørgensen, S. R. Petersen, M. Laurila, J. Lægsgaard, and T. T. Alkeskjold, "Optimizing single mode robustness of the distributed modal filtering rod fiber amplifier," Opt. Express **20**(7), 7263–7273 (2012).

25. S. Ramachandran, J. W. Nicholson, S. Ghalmi, and M. F. Yan, "Measurement of multipath interference in the coherent crosstalk regime," Photon. Technol. Lett. **15**(8), 1171–1173 (2003).

1. Introduction

The successful development of high-power fiber lasers and amplifiers has led to the widespread deployment of this novel technology in scientific and industrial markets [1]. High level output power in these systems is achieved by increasing the effective modal area of fiber-optic elements while simultaneously maintaining diffraction-limited operation [2–6]. Various fiber designs have been proposed and tested [7–12], yielding extremely high pulse energies and peak powers [11,13], in which the single-mode operation of the core region is preserved. Alternatively, very large effective mode areas can be achieved using higher-order mode amplification [7,14,15].

These high-performance fiber designs require new experimental characterization methods to evaluate their modal properties and identify the single-mode (SM) regime. The usual measure of the beam quality in these systems is the so-called M^2-parameter characterizing the physical propagation properties of a beam [16,17]. However, even when this parameter is close to the limiting case of unity, which corresponds to the fundamental Gaussian beam, SM operation is not necessarily guaranteed [18]. Therefore, new alternative methods, which can reliably reveal the modal content of waveguides, are currently under active development.

One such method, called spatially and spectrally (S^2) resolved imaging [19,20], relies on the spectral analysis of the interfering modes guided by the fiber. This method has proved useful in several cases, but it has several important limitations. In particular, the method relies on the use of a reference mode, typically the fundamental mode, when the interference signal is analyzed. Therefore, a reasonable estimate of the relative power content of different modes can be obtained only if one of the modes carries a significant fraction of the energy, and the method fails to characterize the cases where multiple modes have similar power levels. Also, this method requires a spectral range broad enough to detect several interference beatings, typically at least 3 or 4 ones. This becomes problematic for very large mode area fibers where one spectral beat period is 18-30 nm and the length of the fiber is usually limited to about one

meter. A broadband or tunable seed sources delivering close to or over a 100 nm spectral range, necessary in such cases, are not widely available. Real-time determination of modal content is also possible with the correlation filter method [21]. However, this method requires prior knowledge of the modes in the fiber, and thereby modal reconstruction becomes challenging for complex fiber designs. Fortunately, there is an alternative waveguide characterization method, the so-called cross-correlated (C^2) imaging [22,23], free of these limitations: it does not require the use of one of the fiber modes as a reference or a priori knowledge of the modes.

The C^2 imaging method relies on interference in the time domain between an external reference beam and each of the modes propagating in the test fiber, as a function of the relative group delay. The freedom to independently tailor the properties of the reference beam allows one to measure the modal content, as well as dispersion and polarization of all the test modes. One of the main advantages of C^2 imaging is the ability to resolve modal content for arbitrary modal combinations of the test beam [22,23], and define the polarization properties of each mode. The resolution of C^2 imaging is dictated by the spectral width of the seed source, similar to S^2 imaging, however, practically this limitation is more restrictive for the latter. Indeed, as we briefly mentioned earlier, S^2 imaging requires detection of several mode beatings in the frequency domain to resolve the corresponding time delay of the modes via Fourier decomposition. Such additional processing requires an increased bandwidth compared to that of C^2 imaging, where the measurements are taken in the time domain rendering direct modal reconstruction. This advantage is particularly important for the detection of modes in short large-mode area fiber such as rod type fibers which have relatively small relative group delays. In addition, a relatively low implementation cost and narrow spectral requirements of the seed source (1-10nm) (for example LEDs) make it easy to integrate the method with laser systems operating at 1µm.

In this work, we employ C^2 imaging to study the guiding properties of passive large-mode area photonic bandgap rod fibers of 0.92-m length, having a 60-µm mode field diameter. The fiber design is based upon the idea of distributed mode filtering (DMF) [6], which results in SM and multi-moded (MM) operating regimes, depending on the wavelength. In the SM guiding regime, within a specific wavelength range, higher-order modes (HOMs) couple resonantly to a band of narrowly spaced cladding modes (cladding band), formed by the high index inclusions in the cladding, shown as white circular elements in Fig. 1(b). Outside the resonant coupling regime, the fiber appears either MM or does not guide light in the core. A detailed description of the guiding properties and analysis of the DMF rod fibers has been presented in Refs [6,8,9,24]. Here, we demonstrate and experimentally confirm, for the first time to the best of our knowledge, that resonant mode coupling is the primary mechanism by which these fibers provide SM guidance within specific wavelength ranges and demonstrate the feasibility of the C^2 imaging method for short-length and very large mode area fibers. The SM operation was tested for various offset input coupling conditions, and we report higher-order mode suppression levels greater than 20 dB, even for significantly misaligned configurations.

2. Measurement setup

A schematic representation of our C^2 imaging system is shown in Fig. 1(a). The setup utilizes a standard Mach-Zehnder interferometer. The signal and reference paths are created with a beam splitter and consist of the test fiber and a SM polarization maintaining (PM) reference fiber, respectively. Those paths are imaged onto a CCD camera at the output end of the interferometer after recombination. The interferometer has linear polarizers in both arms to ensure the reliable measurement of the modal power of elliptically polarized light transmitted through the test fiber [23]. A linear polarizer in the signal arm defines the plane of polarization of light coupled into the test fiber. The linear polarizer in the reference path ensures coupling either to the fast or slow axis of the SM PM fiber (PM980XP). We chose a

specific length of 101 cm for the reference fiber to bring the optical path of the reference path within the range of the translation stage used to control the relative optical path of the beams.
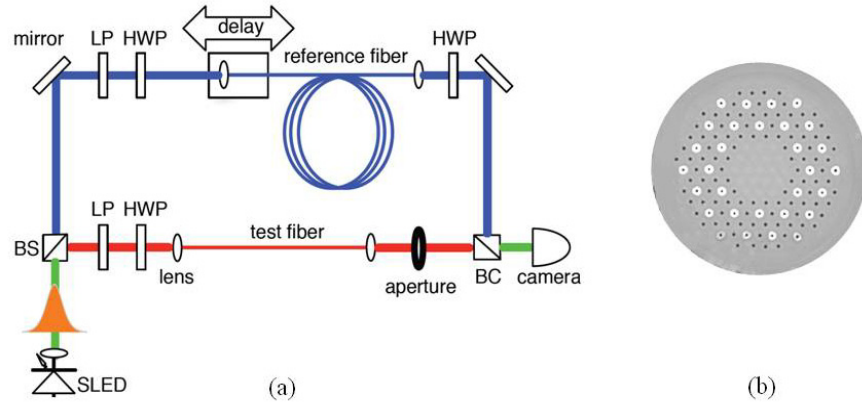

Fig. 1. (a) C^2 imaging setup: SLD – superluminesent diode, BS – beam splitter, BC – beam combiner, LP – linear polarizer, HWP – half-wave plate [23]. (b) Optical micrograph of the DMF rod fiber.

We used a 1050 nm superluminescent SLED as the light source for our experiments. Wavelength tuning is achieved by filtering the source light with an angle-tunable bandpass filter with FWHM of about 10 nm. To avoid scrambling the polarization state, the bandpass was inserted into the signal path before the linear polarizer. The filter has a Gaussian spectral profile and is used at an angle corresponding to a center wavelength of 1040 nm or 1060 nm, as shown in Fig. 2. A near-field image of the fiber under test is obtained using a single (plano-convex) lens with 50-mm focal length which images the fiber output onto a CCD camera. A collimated reference beam is expanded to ensure flatness of the phase front within the imaging range. The beam overlaps spatially with the test fiber image at the image plane of the CCD camera located about 97 cm away from the output end of the test fiber. An adjustable aperture is inserted between the lens and the CCD camera ~23 cm away from the lens. The relative group delay of the reference and the test beam is controlled by a motorized linear translation stage, which changes the length of the interferometer reference arm. A typical experimental run lasted about 30 minutes. The delay stage was moving in steps of ~0.5 μm length within the range of 0.5 mm around interference peaks, and at each delay point an image was recorded. In our setup, there is a slight spatial mismatch of the phase fronts that results from the single-lens imaging and imperfect collimation of the beams. We estimate that the corresponding range of delays over which the beams become phase-matched is significantly lower than the coherence time of our source. Since modal power reconstruction involves averaging over such small time scales, the effect is negligible. When analyzing the cross-correlation traces, we followed the mathematical routines and theory of C^2 imaging developed in [22,23].
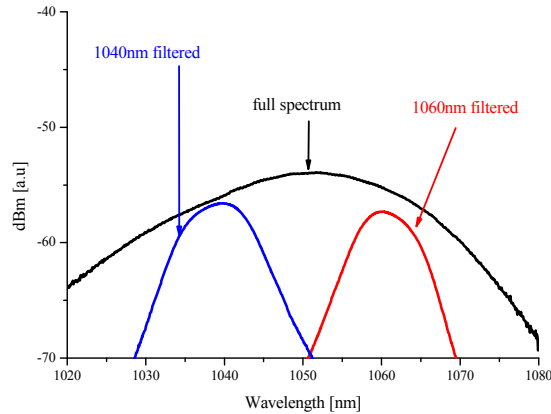
Fig. 2. Measured input spectra used for different C[2] imaging measurements (pick-up fiber HI1060).

The cross-correlation signal $P(x, y, \tau)$ recorded by the CCD camera,

$$P(x, y; \tau) = \sum_m p_m G_{mr}^2 (\tau - \tau_{mr}) I_m(x, y), \qquad (1)$$

is a function of the position (x, y) in the imaging plane and the differential time delay τ_{mr} between each of the modes m and the reference mode r. The signal is obtained by the summation over vertical and horizontal linearly polarized states of the reference beam to account for the possibility of elliptically polarized modes propagating in the test fiber. The time delay $\tau = d/c$, where c is the speed of light in vacuum, is controlled by the position of the translation stage d. The stack of the images $P(x, y; \tau)$ encodes the modal power p_m and the modal intensities $Im(x,y)$ the two quantities of prime importance in our study.

The behavior of $G_{mr}(x, y)$, the magnitude of the coherence function, is dictated by the spectral properties of the seed source, and also by the relative dispersion of the mode m and reference beam r [22,23]. The dispersive broadening of the signal can be compensated by adjusting the length of the reference fiber [22]. When the effects of dispersion are negligible, either due to dispersion-compensation or when the seed source is narrow enough to ignore dispersive effects, the mutual coherence function is characterized by a finite extent in the time domain that is inversely proportional to the spectral bandwidth of the source. This property allows one to separate the modes, when they are characterized by sufficiently large differential group delay. As a result, the modal intensity and the power of every individual mode can be measured. The modal power is encoded in the net C[2] trace, which is obtained by averaging the cross-correlation signal over the imaging plane, taking into account the normalization of the modal intensity.

3. Modeling of C[2] imaging traces of DMF rod fiber

The tested DMF rod fiber is characterized by strong dependence of modal content on the wavelength. The SM guidance regime, most important for practical considerations, is defined by the range of wavelengths where the core power overlap of the fundamental mode (FM) exceeds 80% and, at the same time, the overlap of HOMs is below 50%. Otherwise, the guidance is characterized as MM or leaky. This simple criterion has proved very useful for fabrication of DMF rod fibers [24]. We used a finite-element-method solver to simulate the power overlap ratio in the core of the DMF rod fiber design for the relevant modes, shown in Fig. 3. According to the simulations, the DMF rod fiber design has SM guidance for the wavelengths between 1022 and 1045 nm, and is multimoded outside that spectral range,

supporting HOMs -$LP11_1$, $LP11_2$ $LP11_3$. We considered only the asymmetric modes, since they are most relevant in the experimental situation. Figure 3 shows the simulated vertical components of the electric field profiles for different modes in the SM and MM guiding regimes. The field distributions of these modes are similar to that of a LP11 mode [24], which explains our nomenclature. The field profiles, calculated within the SM guidance regime, illustrate the working principle of DMF rod fiber. In particular, the HOMs effectively couple out from the core to the cladding band and, thus effectively become the cladding modes. These modes are guided either in the resonator elements or inside the cladding structure. The profile of $LP11_3$ mode in Fig. 3 clearly demonstrates this behavior.
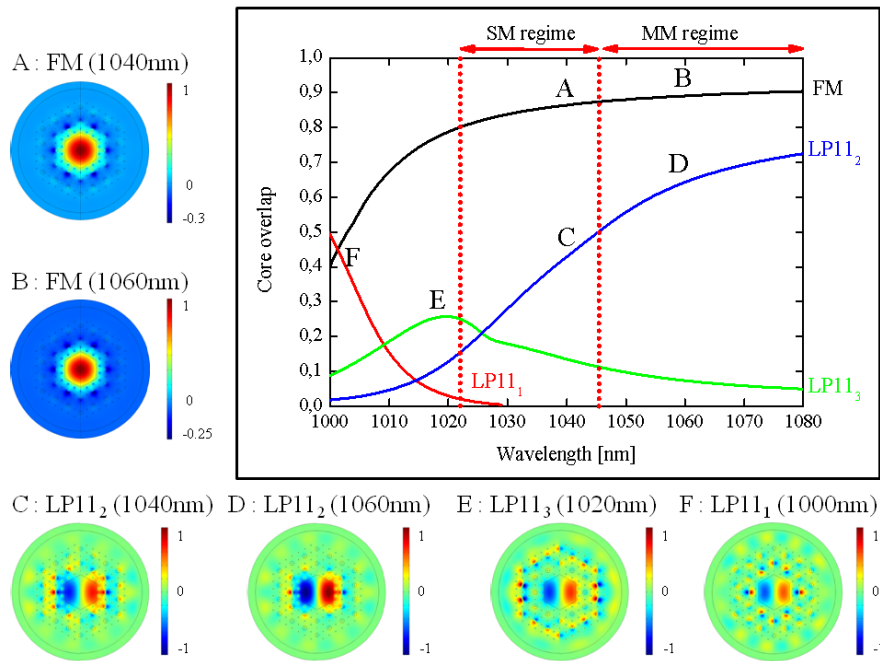

Fig. 3. Simulated core overlap ratio (power) of different modes in the DMF rod fiber. The most relevant modes are shown in SM and MM guiding regimes. Insets illustrate the simulated electric field profiles (y-components) of different modes at specific wavelengths.

We modeled C^2 imaging traces for a specific photonic crystal fiber (PCF) rod design employing distributed mode filtering to estimate the limits of time-delay resolution and understand the ability of the method to probe the modal content of these fibers. Simulated effective refractive indices (n_{eff}) of the modes in the DMF rod fiber are shown in Fig. 4. From the simulated n_{eff} the net C^2 trace in Fig. 5 has been modeled for a specific design of the rod fiber at λ = 1040 nm for a source with Gaussian spectrum with a full width half maximum (FWHM) of 10 nm (spectrum shown in Fig. 5 inset). At this center wavelength the rod fiber operates in the SM regime and supports propagation of the FM and two HOMs, $LP11_2$, and $LP11_3$ - characterized by the relative group delays and dispersion properties obtained from our simulations of the fiber design. The $LP11_1$ mode is neglected due to its low core overlap ratio at 1040 nm. The dash-dotted line represents the coherence function in the case of the ideal dispersion-compensation of all the modes. For this simulation, we have assumed that each of the HOMs has 1% of the total power, which translates to mode suppression at the 20-dB level, as the peak values of the dash-dotted line indicate. The positions of the peaks define the relative group delay of the modes with respect to the FM. Dispersion effects lead to the noticeable broadening of the peaks, resulting in the C^2 trace shown as a solid line.
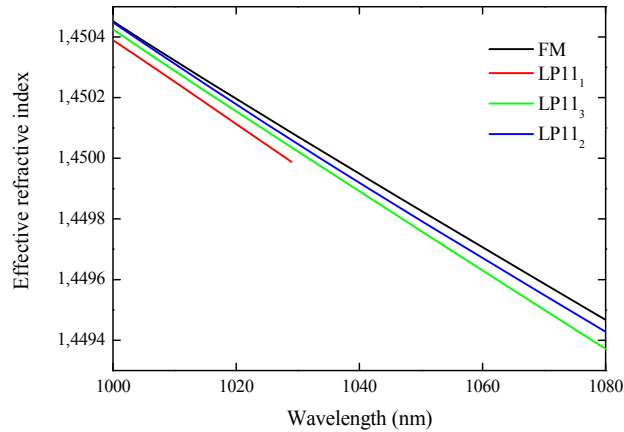
Fig. 4. Simulated effective indices as a function of wavelength for the experimentally relevant modes of the DMF rod fiber.

Simulations of the fiber design used in our experiments, same as in Fig. 3, indicate that in the SM guiding regime at a center wavelength of $\lambda = 1040$ nm, an offset coupling mainly excites two HOMs - $LP11_2$ and $LP11_3$ with average group delay differences of ~1.2 ps/m and ~2.9 ps/m, with respect to the FM, as shown in Fig. 5. At a longer wavelength of 1060nm where the rod fiber is in the MM regime, $LP11_2$ is separated by the group delay value of just ~0.6 ps/m, as Fig. 6 illustrates. The simulations done with Gaussian spectral profiles demonstrate that, at 1040 nm, the $LP11_2$ mode can be clearly resolved in the C^2 imaging trace, as shown in Fig. 5. In contrast, at the wavelength of 1060 nm, due to a smaller group delay, the LP11 mode appears as a shoulder superimposed on the fundamental mode, as seen in Fig. 6.
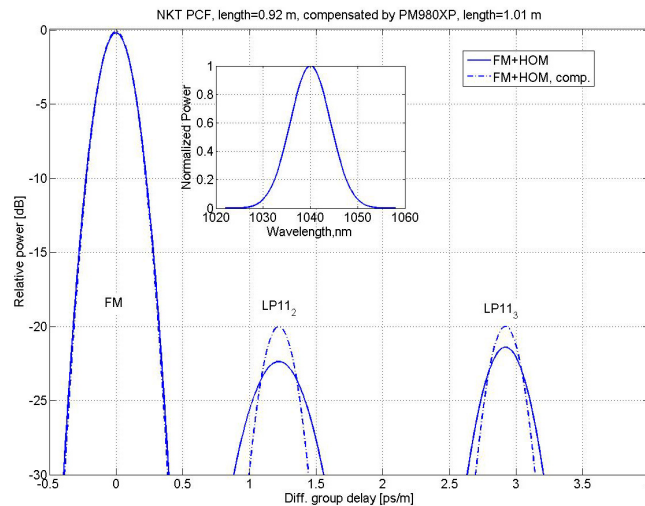

Fig. 5. Simulated C^2 imaging trace of the DMF rod fiber at 1040 nm (98% in the FM, 1% in every of the two HOMs): solid line represents a trace accounting for the dispersion of the modes, dash-dotted line depicts the trace with digitally compensated dispersion. Inset: Gaussian spectrum centered at 1040 nm with FWHM = 10 nm, used in the simulation.
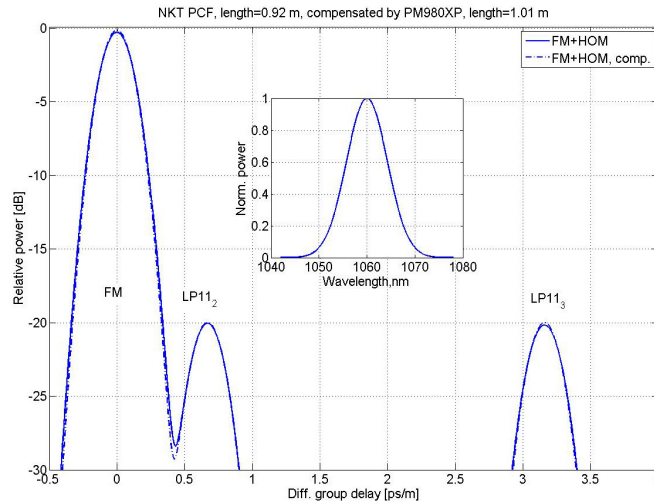
Fig. 6. Simulated C^2 imaging trace of the DMF rod fiber at 1060 nm (98% in the FM, 1% in every of the two HOMs): solid line represents a trace accounting for the dispersion of the modes, dash-dotted line depicts the trace with digitally compensated dispersion. Inset: Gaussian spectrum centered at 1060 nm with FWHM = 10 nm, used in the simulation.

For our simulations and experiments, we have deliberately chosen relatively narrow spectra (FWHM = 10 nm) centered at 1040 nm and 1060 nm. An input signal with wider spectral range would certainly lead to narrower and better resolved temporal features representing the HOMs, but at the same time the broader source would cover both the SM and MM regimes, confusing their relative contribution, see Fig. 3.

4. Experiments

The tested DMF rod fiber had a mode field diameter of 60 μm and length of 92 cm. The end facets of the rod fiber were collapsed within ~200 μm of its flat-cleaved facet. This fiber, characterized by a single cladding structure, is designed and measured to be SM within the wavelength range from 1030 nm to 1050 nm, The exact boundaries of SM regime, difficult to measure experimentally, are estimated with ± 5 nm uncertainty. The fiber design has the parameters of the simulations. Slight differences of the simulated and observed SM regime are possibly caused by manufacturing variations of the fiber parameters. At wavelengths longer than 1050 nm, the fiber becomes MM and, in addition to the fundamental mode, it supports HOMs that are not coupled to the cladding band.

4.1 Input coupling conditions

We evaluate the SM operation of DMF rod fibers at different input coupling conditions by analyzing the corresponding C^2 imaging traces. One expects that offset coupling would result in the appearance of HOMs in the trace, and that their relative contributions should increase as the offset is increased. To analyze these effects in our experiments, we adopted the following procedure. First, the optimal input coupling condition, controlled by the position of the input lens, is identified, in which the C^2 trace reveals the highest fundamental mode content. This content was visually determined by looking at the intensity distribution of the near-field image of the output beam and verified by analyzing a C^2 imaging trace. Then, the input beam is shifted in either the horizontal or vertical direction by the amount specified as $x/y_{\mu m}$, where x and y stand for the horizontal or vertical direction of the offset coupling, respectively. The input beam is moved by the distance (in μm) as measured from the position of optimal input coupling. We limit the displacements to 30 μm in either direction, since, at

larger values, the input light dominantly couples to the cladding band of the fiber, and the core-to-clad intensity ratio decreases to a point where analysis of the core modes becomes meaningless. Specifically, at the 30 μm offset coupling, less than half of the light couples to the core modes of the fiber.

In the SM regime, HOMs within the core resonantly couple to the cladding band and are guided either by the resonator elements through the length of the rod fiber or by the cladding modes which leak away. The coupling between the core and the resonator elements at offset coupling was observed in the near-field images of the fiber output, as evidenced by the appearance of small intensity peaks on top right of Fig. 7 (c) and at the bottom of Fig. 7 (e). These peaks identify the resonator elements in the cladding and prove the coupling of these elements to the core. To support this observation, in some of the experiments we have also used an aperture to remove most of the cladding light with large transverse wave numbers $k\perp$. According to our estimates, an aperture of 2 mm in diameter does not perturb the core

light, while blocking the cladding light propagating with the angles $\dfrac{\Delta k \perp}{k} \geq 1.5 * 10^{-3} \approx 0.08°$.

Thus, with the help of the aperture we could separate the mode content of the core from that of the cladding. In our experiments, the aperture has slightly disturbed the core light, possibly due to imperfect alignment of the aperture along the optical axis of the beam, as follows from a comparison of Fig. 7 (a) and Fig. 7 (b).
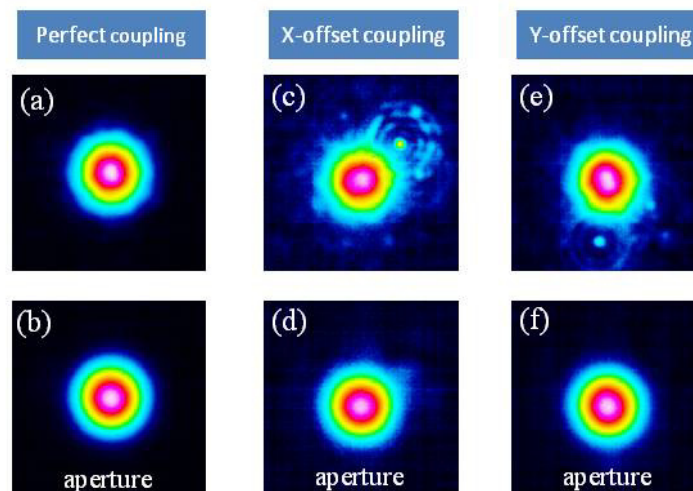

Fig. 7. Near-field images of three different coupling conditions: (a), (c), (e) – without filtering by the aperture, (b), (d), (f) – filtered by the aperture. Images are recorded in the SM regime of the DMF1040 fiber at the wavelength of 1040nm. The offset coupling conditions were x_{30} in (c), (d) and y_{30} in (e), (f), respectively. The small intensity peaks at the top right in (c) and bottom in (e) identify the resonator elements which guide the coupled HOMs from the core to the cladding band.

4.2 Experimental results in single-mode regime

The SM guiding of the DMF1040 was tested at the central wavelength λ = 1040 nm with spectral FWHM = 10 nm, as shown in Fig. 2. According to our simulations at this wavelength the rod fiber appears SM. At the perfect input-coupling condition, the corresponding C^2 trace has two peaks, one corresponding to the fundamental mode, as confirmed by the reconstruction, and another one apparently corresponding to the cladding band, see Fig. 8. Indeed for the latter, the modal reconstruction demonstrates a feature of small relative intensity in the core region, with the size smaller than the FM on top of a noisy background (the boundary of the core is specified by the white dashed line forming a circle). The

reconstructed images were obtained by integrating over portions of the two peaks visible in the C^2 trace, as described in Refs [22,23]. The reconstructed images of the LP01 and cladding modes in Fig. 8 are normalized: the red color corresponds to the maximum and the blue color to the minimum value of the modal intensity. However, these features disappear from the C^2 trace and the reconstructed image when an aperture is applied, as Fig. 8 illustrates.
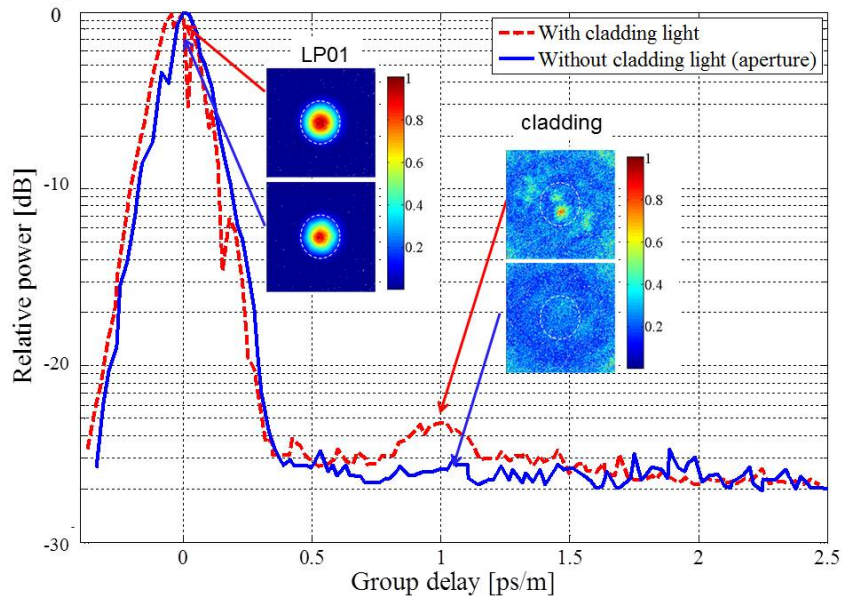

Fig. 8. C^2 trace of the DMF1040 fiber measured at the wavelength of 1040 nm, with and without the aperture, under the perfect coupling condition. The insets show the reconstructed mode images.

The resonant coupling behavior between the core and cladding band becomes evident when the input coupling is deliberately misaligned. According to the fiber design, one expects that thus-excited HOMs are effectively coupled to the cladding band, and C^2 imaging verifies this expectation. Specifically, in Fig. 9, we illustrate C^2 traces obtained at one specific horizontal offset coupling (x_{30}) position. A measurement without the aperture shows a relatively large contribution of HOMs at a differential group delay of ~1 ps/m, which agrees quite well with our simulations (1.2 ps/m) in Fig. 5. However, this mode is characterized by small-scale intensity variations extending beyond the core, see Fig. 9, which indicates that it is not a confined core mode. The bright spot on the left of the core (same direction as the offset coupling condition was) in Fig. 9 corresponds to one of the high-index resonators in the cladding structure. This measurement suggests that a HOM in the core is coupled to the cladding band and then guided in the resonator elements and in the cladding region, generating intensity variation both inside and outside the core. After we apply an aperture the height of the peak in the C^2 trace decreases. The mode profile reconstruction shows a weak HOM and a featureless background noise in the cladding. Our simulations in Fig. 5 also predict other LP11 mode at an average group delay of ~2.9 ps/m, but in the experiments we did not observe this mode even under the extreme offset coupling conditions, presumably due to poor spatial core overlap (see Fig. 3). Interestingly, Fig. 9 also reveals an LP11 mode at a differential group delay of about ~0.5 ps/m, as confirmed by the analysis and mode reconstruction of the corresponding peak.
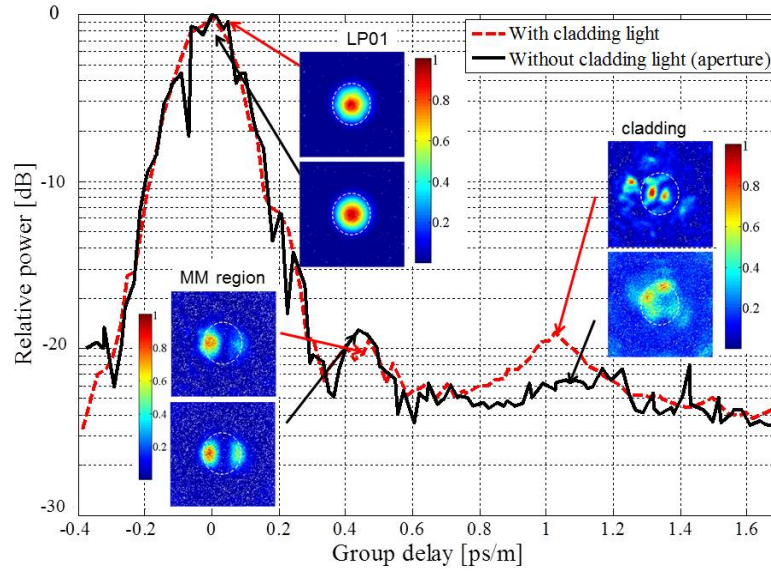
Fig. 9. C² trace of the DMF1040 fiber measured at the wavelength of 1040 nm, with and without the aperture, under X-offset coupling condition. The insets show the reconstructed mode images.

This mode is suppressed 19.5 dB below the fundamental mode. Our simulations of the fiber, performed at 1040 nm (see Fig. 5), seem to disagree slightly with our observations. However, the presence of this mode is in fact the result of a weak spectral overlap of our seed source with the MM regime located at 1060 nm in Fig. 6. Indeed, the spectrum measured at the output of the fiber shows the oscillatory behavior resulting from modal interference at wavelengths exceeding 1050 nm, well inside the MM guiding region, as Fig. 10 illustrates.
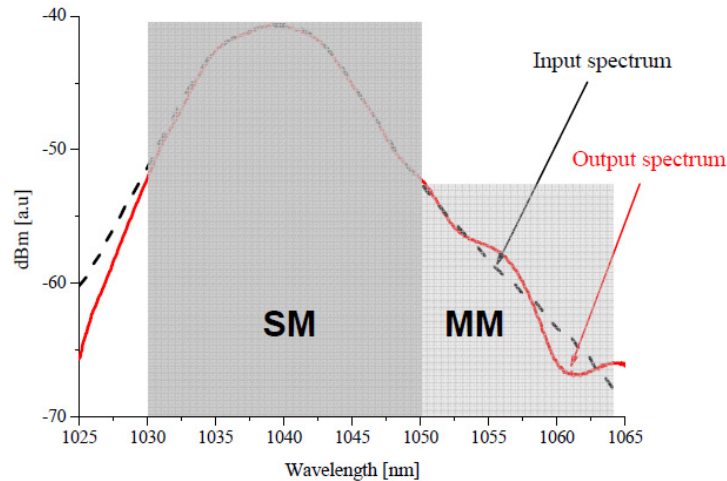

Fig. 10. Input and output spectra of the DMF1040 fiber recorded at the central wavelength of 1040 nm. The output spectrum shows a beating pattern above 1050 nm, outside of the single-mode guiding region of the DMF1040 fiber. The modal content of this mode is measured by C² imaging.

HOMs are slightly more pronounced in the fiber when offsetting input coupling in the y-direction (y_{30}), see Fig. 11. The reconstruction of the peak at ~1.1 ps/m indicates that an LP11 mode is present and is suppressed 20 dB below the FM. Similar to the case observed with offsetting input coupling in the x-direction, a measurement without an aperture shows weak intensity variations around the core (at the group delay of ~1.1ps/m), which indicate the coupling from the core modes to the cladding band. In addition, a HOM at ~0.45 ps/m is visible due to the signal spectral overlap with the MM region. Figure 11 summarizes C^2 imaging measurements performed on the DMF1040 using various offset coupling conditions.

We conclude that even under severe offset couplings (x_{30} or y_{30}) the tested fiber operates in the SM regime with only a small contribution of LP11 mode inside the SM regime, which is suppressed 20 dB below the FM.
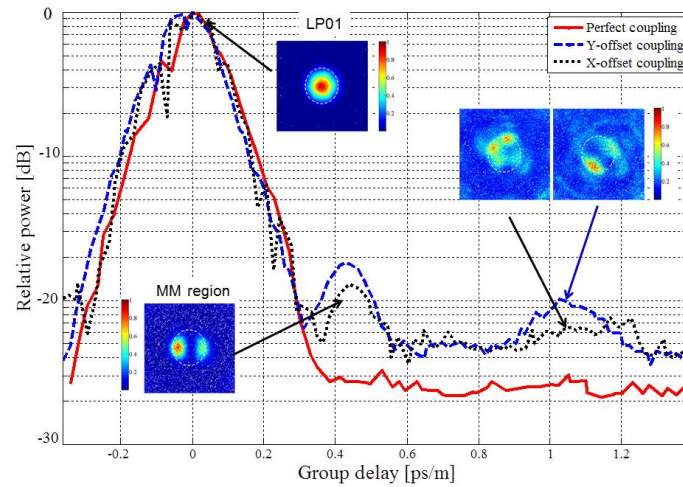

Fig. 11. Summary of different C^2 measurements carried out on the DMF1040 fiber with different coupling conditions (without cladding light) at the wavelength of 1040 nm.

4.3 Experimental results on MM regime

The DMF1040, that was shown to be SM in the 1040 nm wavelength range (see previous section), was also tested at the MM regime at $\lambda = 1060$ nm with FWHM of 10 nm, see Fig. 2. By careful alignment of the input beam, we seemingly excite only the fundamental mode, as the perfectly symmetric output image demonstrates, in the inset of Fig. 12. However, in contrast to the observed near-field image, the C^2 trace in Fig. 12 indicates significant contribution of $LP11_2$ mode to the modal power. Indeed, image reconstruction identifies that the LP01 and $LP11_2$ modes dominate light propagation in the fiber. We note that the $LP11_1$ and $LP11_3$ modes are not observed in our experiments due to their low core overlap ratio at 1060 nm, see Fig. 3. The LP11 mode is suppressed by about 14 dB below the FM. Also, according to our measurements, the rod fiber maintains the state of the linearly polarized input signal, so that no other polarization modes are observed at the fiber output.
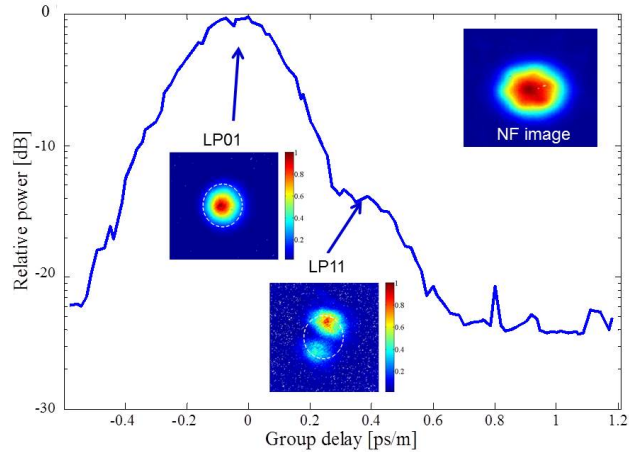
Fig. 12. C^2 trace showing the total power of all the modes obtained from the envelope function of C^2 trace measured at the wavelength of 1060 nm, at optimal coupling, without aperture. The LP11 mode has −14 dB less power than the fundamental mode (LP01). The inset shows the measured NF image of the fiber output. The white dotted circle identifies the core region in the reconstructed mode images.

As expected, when offsetting the input signal, the fiber enters MM regimes of operation. Even though the two modes propagating in the fiber have a small differential group delay, C^2 imaging is still capable of resolving the modes that appear as the two peaks in Fig. 13. The MM behavior identified by C^2 imaging is also confirmed by the analysis of the output spectrum shown in the inset of Fig. 13: the oscillatory component in the spectrum indicates interference of the modes. While simple methods have been used to analyze spectra, similar to the ones shown here, to quantitatively measure modal discrimination [25], unique identification of the modes involved is difficult to obtain with these previous techniques.
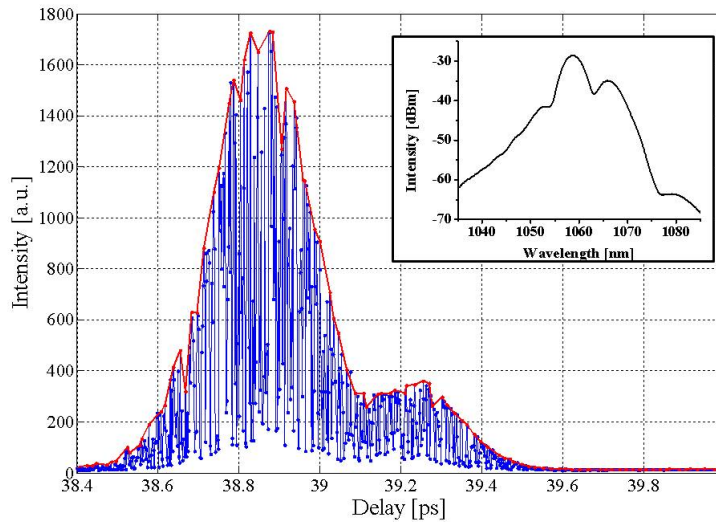

Fig. 13. Example of C2 trace of the DMF1040 fiber at the wavelength of 1060nm (offset coupling condition x_{20}, no aperture). The red line represents the envelope of the trace (averaged over 8 points). The inset shows a beating pattern in the output spectrum.

The offset input coupling along x- and y-directions can lead to strong excitation of the LP11 mode such that, in extreme cases, this mode carries almost 50% of total power in the core, as verified by C^2 imaging. Figure 14 summarizes the characteristic behavior of the fiber for different coupling conditions. Also illustrated in the insets are the corresponding reconstructed mode images. Slight asymmetries of the reconstructed (LP_{11}) images are due to imperfect alignment conditions of the reference and signal beams.
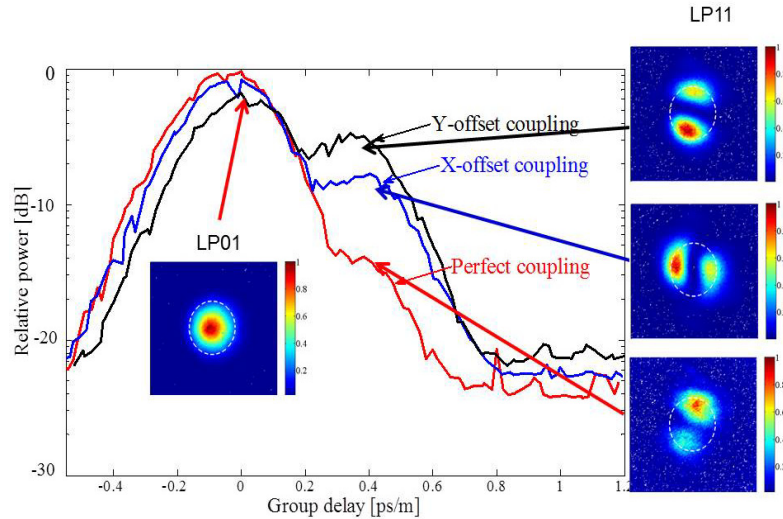

Fig. 14. Summary of different C^2 measurements of the DMF1040 fiber in the multimode region (at 1060 nm) using different coupling conditions: perfect, x_{30} and y_{30} (all done without the aperture). The insets show the reconstructed mode images.

5. Discussion of C^2 imaging results

Using C^2 imaging we have observed the resonant coupling between core and cladding band of the DMF rod fiber. Specifically, in the SM regime, offset input coupling conditions caused the resonant coupling of an excited LP11 mode to the cladding band. By contrast, when the same fiber was tested in the MM regime, such coupling was not observed. In this case C^2 imaging could not identify spatial intensity variation outside the core region indicating effective coupling between the core and the resonator elements.

We used a relatively narrow spectral source with the spectral range (FWHM) of about 10nm to resolve the modes of the DMF rod fiber, yet the high sensitivity of C^2 imaging method enables the detection of LP11 modes resulting from the spectral overlap of the source with the MM regime of operation of the fiber. This is especially visible when the experiments are performed in the SM regime of the fiber (see the discussion of the experiment at 1040nm). One could avoid this effect by using an even narrower source, but in this case the temporal resolution becomes lower due to the broadening of the cross-correlation traces, which would render the modal content measurements impossible. It is desirable, therefore, to employ narrow sources with some appreciable smooth spectral width to avoid artifacts, such as the characteristic sinc-like "ringing" due to the sharp spectral edges, possibly those with the spectral shape decaying faster than a Gaussian function.

In our C^2 imaging measurements, the background noise level limits the range of modal weight measurements. At perfect input coupling conditions the background noise level is estimated to be suppressed by 28 dB compared to the signal peak intensity but this suppression reduces to 26 dB for offset coupling conditions due to a reduced power transmission.

Although we performed our C^2 imaging measurements on a passive DMF rod fiber, we believe that the methods discussed here can be also employed for the studies of active fibers. This is hard due to signal absorption at 1030 nm which decreases the signal-to-noise ratio. If the doping level was high enough, all signal light guided within the core would be absorbed along the fiber length, thereby rendering C^2 imaging impossible. One way to get around the problems arising from absorption is to operate the active medium in a transparent regime, by, for example, supplying the signal light with sufficient gain. Thus, if gain or thermo-optic shifts of the refractive index profile are negligible, it is conceivable that C^2 imaging may be feasible even in high-power amplifiers.

6. Conclusions

We have experimentally analyzed the modal content of a passive single-mode bandgap distributed mode filtering (DMF) rod fiber by operating the rod fiber in a SM guiding regime under different input coupling conditions using the cross-correlated (C^2) imaging method. Using this method, we have identified and verified the modal filtering of higher-order modes (HOMs) via resonant coupling of the modes to the cladding band. This mechanism is responsible for single-mode operation of DMF rod fibers. In the single-mode regime, we measured a relatively high amount of HOMs in the resonator elements in the cladding due to the resonant coupling excited by offsetting input coupling conditions. We have shown the capability of C^2 imaging in resolving modal content of very large mode area photonic crystal bandgap fibers. We evaluated the single-mode properties of the DMF rod fiber in different guiding regimes and reported a single-mode regime where HOMs are suppressed by more than 20 dB below the peak intensity of the fundamental mode. Most significantly, our technique helps experimentally reveal the resonant coupling mechanism between the core and cladding band that is a basis for a large class of LMA fiber designs for future high-power fiber laser systems.

Acknowledgments